Self-consistent decay of superfluid turbulence

Carlo F. Barenghi* and David C. Samuels†
Department of Mathematics, University of Newcastle, Newcastle NE1 7RU, England
(Received 23 February 1999)

Recent experiments have shown that the isothermal turbulent motion of helium II is very similar to classical turbulence. This regime is characterized by a strong coupling between the superfluid vortex tangle and the normal-fluid component. To study this coupled regime we develop an approach to compute the evolution of the vortex tangle. Its key feature is that it is *dynamically self-consistent*, unlike previous approaches, because it takes into account the back rection of the vortex tangle onto the normal fluid. We implement this approach and study a model system which, although very idealized, gives some insight into the transfer of energy between the two fluid components. [S0163-1829(99)00526-3]

I. BACKGROUND

The evidence from some recent experiments is that the turbulent motion of liquid helium II can be described well using the same rules of turbulence as in a classical fluid (such as water, air, or helium I). These experiments include measurements of mass flow rates and pressure gradients along pipes,[1] measurements of the circulation of large scale turbulent vortex rings,[2] visualization of turbulent Couette flow,[3] measurements of the decay of vorticity in turbulence generated by towing a grid,[4–6] and measurements of energy power spectra in turbulence continuously excited by rotating blades.[7]

These results are at first surprising because helium II is a quantum fluid, and, at least at small velocities, usually behaves in a way which is very different from a classical Navier-Stokes fluid. The difference arises from the existence in helium II of two separate but copenetrating fluid components: the superfluid (with density ρ_s and zero viscosity) and the normal fluid (with density ρ_n and finite viscosity μ). The relative proportion of normal-fluid density and superfluid density to the total density of helium II $\rho=\rho_s+\rho_n$ is determined by the temperature T. At absolute zero helium II is entirely superfluid ($\rho_n/\rho=0$, $\rho_s/\rho=1$); increasing T increases ρ_n, until the lambda transition is reached at $T=T_\lambda=2.172\,\mathrm{K}$, and helium II becomes entirely normal ($\rho_n/\rho=1$, $\rho_s/\rho=0$). This two-fluid theory explains well many nonclassical flow phenomena which occur in helium II, such as second sound, thermal counterflow, and superleaks, as well as their strong temperature dependence.

Unlike the laminar flows traditionally studied by the two-fluid theory, the experiments of Refs. 1–7 consider flows which must be very turbulent. A convenient measure of the turbulence intensity is provided by the Reynolds number $R=UL/\nu$, where U and L are speed and length scales and $\nu=\mu/\rho$ is the kinematic viscosity. Typically we have $R\approx10^6$ for the pipe flow experiments,[1] $R\approx10^4$ for the vortex ring experiments,[2] and $R\approx10^5$ for the towed grid[4,5,6] and the rotating blade experiments.[7] Now we know that if helium's speed exceeds a small critical value a large number of quantized vortex filaments appear in the superfluid and form a dense, disordered tangle. The vortex filaments scatter[8] the thermal excitations (phonons and rotons) which make up the normal fluid, and thus introduce a mutual friction force[9] which couples the normal fluid and the superfluid. The apparent classical behavior of helium II when turbulent must therefore be associated with the vortex filaments. The experiments indicate that the mutual friction coupling can be so strong that the normal fluid and the superfluid lock together, yielding effectively a single fluid of density ρ, a phenomenon referred to as *vortex coupled superfluidity*.[10] A striking feature of the phenomenon is its temperature independence, which is unusual when studying helium II flows. For example the measurements of vorticity decay[4–6] and of the energy spectra[7] give the same result in the observed range $1.4\,\mathrm{K}<T<T_\lambda$. Note that at temperatures as low as 1.4 K there is too little normal fluid left ($\rho_n/\rho=7.5\%$) to make that fluid component solely responsible for the observed classical behavior.

Besides being interesting physics *per se*, vortex coupled superfluidity opens the possibility of using helium II to study issues of classical turbulence: an example is the recent work of Stalp, Skrbek, and Donnelly[6] to model spectra of decaying turbulence from data taken in helium II. There may also be the possibility of developing new instrumentation to measure turbulent vorticity using the second-sound technique.

II. THE KINEMATIC APPROACH TO TURBULENCE

On the theoretical side very little is known about high Reynolds numbers helium II flows and one must still concentrate on understanding the basic physical mechanisms involved. So far the most fruitful approach to study the behavior of the superfluid vortex tangle was pioneered by Schwarz.[11] He showed that if a vortex filament is specified in parametric form $\mathbf{s}=\mathbf{s}(\xi,t)$ where ξ is arclength and t is time, then the velocity of a given point $\mathbf{s}$ of the filament depends on imposed superflow $\mathbf{v}_s$ and normal flow $\mathbf{v}_n$ in the following way:

$$\frac{d\mathbf{s}}{dt}=\mathbf{v}_s+\mathbf{v}_i+\alpha\mathbf{s}'\times(\mathbf{v}_n-\mathbf{v}_s-\mathbf{v}_i). \tag{1}$$

Here a prime denotes derivatives with respect to arclength, B is a known[9] temperature-dependent coefficient which describes the friction between the vortex filaments and the nor-

mal fluid, and $\alpha=\rho_n B/(2\rho)$. In writing Eq. (1) the small transverse part of the friction force has been neglected for simplicity. The quantity $\mathbf{v}_i$ is the velocity which the vortex filament induces onto itself because of its own curvature, and is determined by the Biot-Savart integral

$$\mathbf{v}_i(\mathbf{s})=\frac{\kappa}{4\pi}\int_{\mathcal{L}}\frac{(\mathbf{z}-\mathbf{s})\times\mathbf{dz}}{|\mathbf{z}-\mathbf{s}|^3}, \tag{2}$$

where $\kappa=9.97\times10^{-4}\,\mathrm{cm}^2/\mathrm{s}$ is the quantum of circulation and the integral extends over the entire vortex configuration $\mathcal{L}$. Schwarz's approach consists in discretizing an initial vortex configuration into a number N of points and then using Eqs. (1) and (2) to move each individual point. The computer code must allow for a variable time step and a variable N; more points and better temporal resolution are necessary if, during the time evolution, a region of tight curvature appears along a vortex line. The code must also allow for vortex reconnections[12] which take place when two vortex filaments get very close to each other.

The practical limitation of Schwarz's approach arises from the calculation of the Biot-Savart integral (2), an operation which increases quadratically with the number of points. Schwarz's remedy was to use the local induction approximation to the exact Biot-Savart law, which is

$$\mathbf{v}_i(\mathbf{s})=\frac{\kappa}{4\pi R}\ln\left(\frac{R}{a_0}\right)\mathbf{b}. \tag{3}$$

Here R is the local radius of curvature, $a_0\approx10^{-8}\,\mathrm{cm}$ is the vortex core parameter (the region from the center of the vortex over which the amplitude of the quantum-mechanical wave function drops from its bulk value to zero), and $\mathbf{b}$ is the local unit vector in the binormal direction $\mathbf{s}'\times\mathbf{s}''$. The calculation of $\mathbf{v}_i$ using Eq. (3) grows only linearly with with N, which makes it possible to study intense vortex tangles which contain a very large number of points. The use of Eq. (3) is, however, delicate. The vortex tangles studied by Schwarz arise from turbulent heat flows and they are characterized by being rather homogeneous and almost isotropic; this implies that long-range effects tend to cancel out each other, and in fact Schwarz found that the use of Eq. (3) in place of Eq. (2) is a fair approximation in the problems of conterflow turbulence which he studied. In general, however, long-range effects are important, and the use of Eq. (3) can give misleading results, as we have discovered recently in a study of the evolution of knotted vortex structures.[13] This is why hereafter we choose to use the exact Biot-Savart law (2), and restrict ourselves to the study of low-density vortex tangles.

Schwarz's vortex dynamics approach to the turbulence problem was followed up by Samuels,[14] Aarts and DeWaele,[15] and Penz, Aarts, and deWaele[16] among others,[17] and the technique to perform the calculation, which has rather subtle aspects—such as the desingularization of Eq. (2)—is now standard.

III. DIFFICULTIES OF THE KINEMATIC APPROACH

The drawback of Schwarz's vortex dynamics approach is that it is essentially *kinematic* in character: the driving fields $\mathbf{v}_n$ and $\mathbf{v}_s$ are imposed at the beginning of the numerical calculation and never change. This limitation is present in all work published until now. For example, when studying counterflow turbulence, Schwarz set $\mathbf{v}_n-\mathbf{v}_s$ equal to a constant, proportional to the driving heat flux. Choices of $\mathbf{v}_n$ used in the literature range from uniform flows[11] in periodic boxes or channels, Poiseuille flows,[15] a single vortex tube,[16] and ABC flows.[18] In each case the shape of the profile of $\mathbf{v}_n$ was fixed.

The difficulty of kinematic models becomes apparent, since the normal fluid is viscous, when flows with boundaries are studied, such as channel flows. On one hand it can be argued that $\mathbf{v}_n$ should have a parabolic Poiseuille profile to satisfy the no-slip boundary conditions at the wall; on the other hand one can also argue that the parabolic profile gets so flattened by the friction with the superfluid vortex tangle that a uniform profile may be a better choice. Aarts and deWaele[15] tested both these profiles and, not too surprisingly, they found that the vortex tangle looks very different if $\mathbf{v}_n$ is parabolic rather than uniform.

The same difficulty appears when one tries to determine the normal fluid as a function of a fixed tangle rather than vice versa. This was attempted by Melotte and Barenghi[19] who studied the linear stability of $\mathbf{v}_n$ under the forcing of an imposed homogeneous and isotropic vortex tangle. Their calculation showed that if the vortex tangle exceeds a critical density the Poiseuille profile becomes unstable and possibly turbulent, a transition which would clearly change the vortex tangle itself.

IV. THE SELF-CONSISTENT APPROACH TO TURBULENCE

The aim of this paper is to overcome the difficulty of the kinematic approach. We propose a dynamically *self-consistent* approach which takes into account the back reaction of the vortex tangle onto the normal fluid. The idea consists in letting the normal fluid evolve alongside the tangle of superfluid vortex lines, according to its own equation of motion. In this way the vortex tangle and the normal-fluid profile determine each other in a dynamically self-consistent fashion. For example, in the channel flow problem studied by Aarts and DeWaele, the calculation would start as usual with few superfluid vortex lines to act as seed, while the normal fluid would be initially in the correct parabolic profile to satisfy the boundary conditions; as the vortex tangle develops, the back reaction of the tangle onto $\mathbf{v}_n$ via friction would increase, changing the parabolic profile of $\mathbf{v}_n$. In this way, if the friction is large enough, $\mathbf{v}_n$ may become distorted, flattened, or even turbulent, as argued by Melotte and Barenghi[19] in the context of heat transfer flow.

To implement this approach we consider the equation of the normal fluid, which we assume isothermal and incompressible for simplicity. Neglecting any externally applied superfluid potential flow, this equation is the Navier-Stokes equation modified by the introduction of the friction force:

$$\rho_n\frac{\partial\mathbf{v}_n}{\partial t}+\rho_n(\mathbf{v}_n\cdot\nabla)\mathbf{v}_n=-\frac{\rho_n}{\rho}\nabla P+\mu\nabla^2\mathbf{v}_n+\mathbf{F}, \tag{4}$$

where P is the pressure. Equation (4) must be solved together with the continuity equation

$$\nabla \cdot \mathbf{v}_n = 0. \tag{5}$$

The friction force per unit volume at a given point is[11,14]

$$\mathbf{F} = \frac{\kappa B \rho_n \rho_s}{2\rho} \frac{1}{V} \int_{\mathcal{L}} \mathbf{s}' \times [\mathbf{s}' \times (\mathbf{v}_n - \mathbf{v}_s - \mathbf{v}_l)] d\xi, \tag{6}$$

where the integration is performed over the vortex lines in the volume V around that particular point. Note that until now the calculation of the friction (6) has been attempted for diagnostic reasons only, in the context of kinematic models.

The self-consistent approach consists therefore in solving Eqs. (1) and (2)—which determine the tangle for a given normal fluid—together with Eqs. (4), (5), and (6)—which determine the normal fluid for a given tangle. Essentially, we combine an Euler description of the normal fluid with a Lagrange description of the superfluid tangle.

It is apparent that, in principle, modeling turbulent helium II as a turbulent normal flow coupled to a superfluid vortex tangle is a formidable task of computational fluid dynamics. It is more challenging than the existing numerical simulations of classical Navier-Stokes turbulence, not only because there are more degrees of freedom, but also because of the very localized nature of the friction force (6), which requires many length scales to be resolved. In the next section we shall introduce and discuss a series of approximations which make the numerical task more manageable.

V. THE CALCULATION OF THE FRICTION

When computing the friction force (6) on the normal fluid a difficulty arises as to what should be the volume V over which $\mathbf{F}$ is calculated. Both Schwarz[11] and Aarts and DeWaele,[15] who computed $\mathbf{F}$ for diagnostic reasons, defined V as the entire computational box. This approximation is clearly convenient when making comparison with the experiments: in most cases in fact what can be observed is only the average value of the friction (or of its effect on second sound, for example) integrated over a large region of flow, such as the cross section of the experimental channel. If we followed this approach we would therefore replace $\mathbf{F}(\mathbf{r},t)$ with its spatial average $\langle \mathbf{F}(t) \rangle$. The drawback, of course, is that we would entirely lose any local spatial information about the mutual friction forcing (6). Penz, Aarts, and deWaele[16] attempted to retain some local information by dividing the volume of their circular pipe over which $\langle \mathbf{F} \rangle$ is evaluated into an inner region and an outer region of similar size, thus yielding two values of the forcing. They also time averaged the two values, but this was because of a special feature of the problem which they were studying which need not concern us in general.

From a physical point of view the friction force which a vortex line exerts on the normal fluid acts over a very small, localized region, hence in principle the motion of the normal fluid should be resolved over such a small length scale. In the temperature range $1.4\,\mathrm{K} < T < T_\lambda$ relevant to the experiments most of the friction is caused by the scattering of rotons from the velocity field around the vortex line over a range[8] of a few hundred times a_0. Unfortunately, this range is much too small a length scale to be resolved by existing computers: the study of a realistic situation would require to calculate a flow with length scales ranging over 5 or 6 orders of magnitude (the current numerical simulation of Navier-Stokes turbulence typically use from 128 to 256 mesh points in each direction, leaving a gap of four orders of magnitude!). Some spatial averaging is clearly necessary. Time averaging is not required unless one is interested in problems which involve high-frequency second sound: the reason is that the vortex core is so small that a vortex line has negligible inertia and responds immediately to the friction. If one took into account the finite hydrodynamic mass of the vortex core, then vortex filaments would perform very small amplitude oscillations at the cyclotron frequency $\omega_{\mathrm{cyclo}} \approx \kappa / a_0^2 \approx 10^{13}$ rad/s with negligibly small amplitudes proportional to $v_s / \omega_{\mathrm{cyclo}}$.

The spatial averaging which we have chosen attempts to retain local information about the friction. It consists in averaging $\mathbf{F}$ over a volume V determined by the same spatial mesh size h used in the computation of $\mathbf{v}_n$ itself. What motivates our approximation is that it reduces to a known limit. In fact, if the vortex filaments are spatially ordered and if the vortex line length per unit volume L is large, then our approximation becomes operationally equivalent to the familiar Hall-Vinen-Bekharevich-Khalatnikov (HVBK) equations[20] which are used to describe uniform flows (such as solid-body rotation) or almost uniform but still laminar flows (such as Taylor-Couette flow[21]). The HVBK equations describe the flow induced by the vortex filaments as a continuum, in which a fluid particle (numerically defined by the mesh size h) is a small region threaded by a number of vortex filaments which is large enough to define an averaged vorticity of the superfluid. Physically, it means that the vorticity is spatially organized and that the intervortex spacing $L^{-1/2}$ is much smaller than any length scale in the flow. The existence of the HVBK limit at high L, however, does not mean that we are able to achieve it when implementing our approach. On the contrary, because of the constraints of the computing power available, we are never in a situation in which any region of the flow contains a very large number of vortex lines, more so because we choose to use the computationally expensive Biot-Savart law. Nevertheless, the existence of the HVBK limit makes our approach less arbitrary.

VI. A SIMPLIFIED MODEL OF SELF-CONSISTENT DECAY

To implement the self-consistent approach we consider the simple problem of the decay of a tangle of superfluid vortices coupled together with a decaying normal fluid. This problem is motivated by the measurements of the decay of vorticity created by a towed grid.[4,5,6] Following Schwarz, to simplify the calculation we consider a periodic Cartesian (x,y,z) cubic box of size λ. Even without boundaries, this still leaves us with the numerical complexity of Schwarz's approach with that of a three-dimensional simulation of the Navier-Stokes equation. We introduce therefore the further simplifying assumption that the normal fluid is *two dimensional*, that is to say, although we do allow for motion in the y direction, we assume that all velocity components are independent of y. This assumption makes the model computationally accessible. The model is clearly rather idealized, but this is the initial stage of investigation of the coupled motion of vortex lines and normal fluid. Moreover, we are careful in

the way we proceed: for example, we select special initial conditions [Arnold-Beltrami-Childress (ABC) flows] which have a natural tendency to retain their shape, hence remain two dimensional, and study only decay processes. Since in our model the vortex configuration is not isotropic, the use of the exact Biot-Savart law (2) at the place of the local induction approximation (3) used by others is clearly more consistent and preferable. However, the use of the Biot-Savart law also limits the density L of the tangle which we can study, which adds to the limitations of the model.

The assumption of reduced dimensionality (a three-dimensional vortex tangle interacting with a two-dimensional normal fluid) has never been used in the study of the hydrodynamics of helium II, but is not new in other applications of fluid dynamics. In particular, it has been used with success to study magnetohydrodynamics dynamo action. Noteworthy examples are the Ponomarenko dynamo and the G. O. Roberts dynamo,[22,23] in which two-dimensional fluid motions are studied which are able to generate a three-dimensional magnetic field.

We make the equations of motion dimensionless by calling λ the unit of length and the viscous diffusion time of the normal fluid λ^2/ν_n as unit of time, where the kinematic viscosity is defined as $\nu_n=\mu/\rho_n$. We indicate dimensionless quantities with a star: we write $t^*=t\nu/\lambda^2$, $\mathbf{r}^*=\mathbf{r}/\lambda$, $L^*=\lambda^2 L$, $\mathbf{s}^*=\mathbf{s}/\lambda$, $\mathbf{v}_n^*=\mathbf{v}_n\lambda/\nu$, and $\mathbf{v}_s^*=\mathbf{v}_s\lambda/\nu$. Other choices of time units are possible (for example λ^2/κ), but our choice seems more appropriate since we are interested in a decay process and we want to make comparison to what happens in the limit $T\rightarrow T_\lambda$ in which Eq. (4) becomes the classical Navier-Stokes equation. It must also be noticed that the non-dimensionalization of the equations is not complete because of the existence of the vortex core cutoff parameter a_0 in the desingularization of the Biot-Savart law [or in the local induction approximation, had we used Eq. (3)]. This problem is unavoidable because it is not sensible to base the length scale of the flow on a quantity of atomic dimensions. So, when necessary, we use the correct dimensional value $a_0\approx 10^{-8}$ cm, which corresponds to assuming that $\lambda=1$ cm. Since this is the typical size of an experimental cell and we are concerned only with the argument of a slowly varying logarithmic function, the interpretation of the results should not be much affected.

Neglecting any imposed superflow ($\mathbf{v}_s^*=0$), the dimensionless equation of a vortex filament is then

$$\frac{d\mathbf{s}^*}{dt^*}=\mathbf{v}_i^*+\alpha\mathbf{s}^{*\prime}\times(\mathbf{v}_n^*-\mathbf{v}_i^*), \tag{7}$$

where the self-induced velocity is

$$\mathbf{v}_i^*(\mathbf{s}^*)=\frac{\Gamma}{4\pi}\int_{\mathcal{L}}\frac{(\mathbf{z}^*-\mathbf{s}^*)\times\mathbf{dz}^*}{|\mathbf{z}^*-\mathbf{s}^*|^3}, \tag{8}$$

and Γ is the dimensionless quantum of circulation,

$$\Gamma=\kappa/\nu_n. \tag{9}$$

The dimensionless normal-fluid equations are

$$\frac{\partial\mathbf{v}_n^*}{\partial t^*}+(\mathbf{v}_n^*\cdot\nabla^*)\mathbf{v}_n^*=-\nabla^*P^*+\nabla^{*2}\mathbf{v}_n^*+\mathbf{F}^*, \tag{10}$$

$$\nabla^*\cdot\mathbf{v}_n^*=0, \tag{11}$$

where ∇^* refers to derivatives with respect to x^*, y^*, and z^* and P^* is the rescaled pressure. Since the normal flow is two dimensional it is convenient to introduce a stream function ψ^*:

$$\mathbf{v}_n^*=(u^*,v^*,w^*)=\left(-\frac{\partial\psi^*}{\partial z^*},v^*,\frac{\partial\psi^*}{\partial x^*}\right), \tag{12}$$

which guarantees that the continuity Eq. (11) is satisfied. We also introduce the y^* component of the vorticity

$$\zeta^*=\frac{\partial u^*}{\partial z^*}-\frac{\partial w^*}{\partial x^*}. \tag{13}$$

In this way we have two equations of motion for v^* and ζ^*,

$$\frac{\partial v^*}{\partial t^*}=\frac{\partial^2 v^*}{\partial x^{*2}}+\frac{\partial^2 v^*}{\partial z^{*2}}+\frac{\partial(v^*,\psi^*)}{\partial(x^*,z^*)}+F_y^*, \tag{14}$$

$$\frac{\partial\zeta^*}{\partial t^*}=\frac{\partial^2\zeta^*}{\partial x^{*2}}+\frac{\partial^2\zeta^*}{\partial z^{*2}}+\frac{\partial(\zeta^*,\psi^*)}{\partial(x^*,z^*)}+(\nabla^*\times\mathbf{F}^*)_y, \tag{15}$$

together with a Poisson equation for the stream function,

$$\frac{\partial^2\psi^*}{\partial x^{*2}}+\frac{\partial^2\psi^*}{\partial z^{*2}}=-\zeta^*, \tag{16}$$

where the Jacobian of two functions f and g is defined as

$$\frac{\partial(f,g)}{\partial(x^*,z^*)}=\frac{\partial f}{\partial x^*}\frac{\partial g}{\partial z^*}-\frac{\partial f}{\partial z^*}\frac{\partial g}{\partial x^*}, \tag{17}$$

and the dimensionless friction $\mathbf{F}^*$ is

$$\mathbf{F}^*=\alpha\Gamma\frac{\rho_s}{\rho_n}\frac{1}{V}\int_{\mathcal{L}}\mathbf{s}^{*\prime}\times[\mathbf{s}^{*\prime}\times(\mathbf{v}_n^*-\mathbf{v}_i^*)]d\xi^*. \tag{18}$$

The numerical calculation requires initial conditions for the normal fluid and for the vortex tangle. As the initial condition for the normal fluid we take an Arnold-Beltrami-Childress (ABC) flow.[24] This flow is an idealized model of an eddy, much used in the study of magnetohydrodynamics turbulence and dynamo action.[25] In the context of superfluidity, ABC flows have been used to model turbulence structures of the normal fluid.[18] In general, ABC flows are defined by the Cartesian components

$$u=A\sin(2\pi z/\lambda)+C\cos(2\pi y/\lambda), \tag{19}$$

$$v=B\sin(2\pi x/\lambda)+A\cos(2\pi z/\lambda), \tag{20}$$

$$w=O\sin(2\pi y/\lambda)+B\cos(2\pi x/\lambda), \tag{21}$$

where A,B, and C are parameters. An interesting property of ABC flows is that they are solutions of Euler's equation and when substituted into Eq. (4), in the absence of friction, they decay in time as $\mathbf{v}(t)=\mathbf{v}(0)\exp(-4\pi^2\nu_n t/\lambda^2)$, in which is $\mathbf{v}^*(t^*)=\mathbf{v}^*(0)\exp(-4\pi^2 t^*)$ in dimensionless units. The existence of this precise decay law will prove particularly useful in analyzing the results.

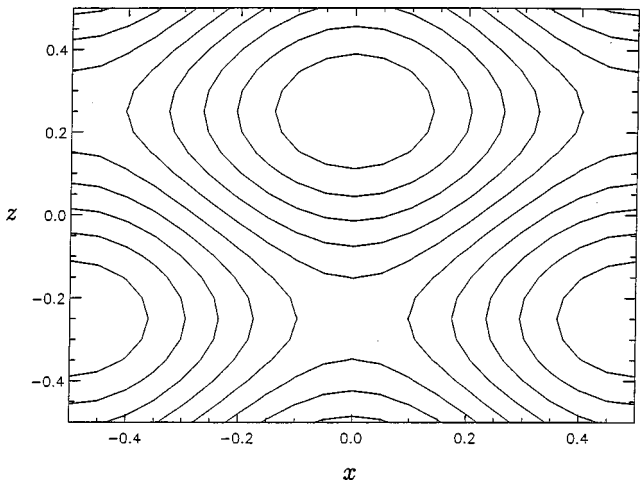

FIG. 1. Contour plot of y component of the ABC normal-fluid velocity.

We obtain a two-dimensional ABC flow by setting $C=0$ and we take $A=B$ for simplicity. In dimensionless form we have

$$u^*=A^*\sin(2\pi z^*), \tag{22}$$

$$v^*=A^*\sin(2\pi x^*)+A^*\cos(2\pi z^*), \tag{23}$$

$$w^*=A^*\cos(2\pi x^*). \tag{24}$$

Figure 1 illustrates the spatial structure of the initial normal fluid.

The initial condition for the superfluid is an arbitrary three-dimensional vortex tangle of some line density L^*. The tangle is created by seeding a suitable two-dimensional ABC flow with a superfluid vortex ring. Driven by the Glaberson instability, the vortex ring develops vortex waves which become unstable, grow, reconnect, and create a vortex tangle which, although three dimensional, has the same average spatial structure of the driving, fixed ABC normal flow, as we showed in a previous paper.[18] Here we stop the calculation before saturation takes place because the use of the Biot-Savart law limits the density of the tangle which we can study. The resulting initial tangle is shown in Fig. 2: the main feature is the spiral structure of the tangle which produces the average superfluid velocity field illustrated in Fig.

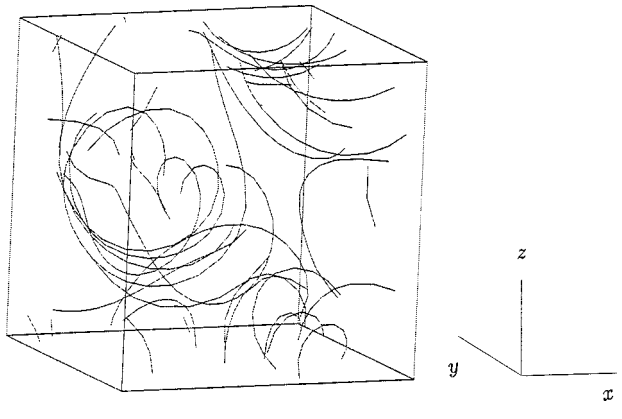

FIG. 2. Vortex tangle created by an ABC flow.

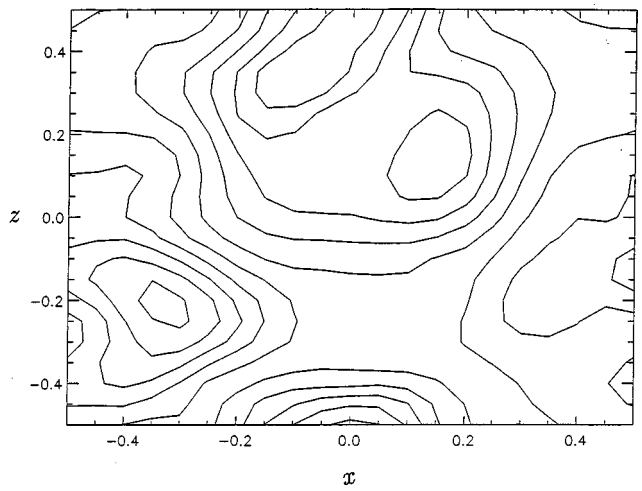

FIG. 3. Contour plot of the average y component of the superfluid velocity corresponding to the tangle of Fig. 2.

3, which must be compared with the related normal fluid of Fig. 1. Note that this calculation to produce the initial tangle is kinematic in character.

In summary, our initial condition consists of a two-dimensional ABC normal flow and a vortex tangle which is two dimensional only in an average sense.

The numerical technique to integrate the motion of the vortex tangle for a given normal fluid has been already described[14,18] in detail, including the tests applied to the computer code. The integration of the normal-fluid equation is performed by subdividing the computational box into a two-dimensional grid of N equally spaced mesh points in each direction, $h=1/N$ being the grid's spacing. The time stepping of the normal fluid is performed using the alternating direction implicit technique for the linear terms and the Adams-Bashforth method for the nonlinear terms. The Poisson equation for ψ is solved using the fast Fourier transform method. The number of mesh points is typically $N=20$. This resolution is typical for similar flows studied in the literature, for example Taylor-Couette flow.[26] The resolution has been tested to obtain the correct decay rates of the ABC flow. At each time step the components of the friction force **F** are computed as described in Sec. V and averaged over the y direction. Because of the computational constraint of the Biot-Savart law, the number of vortex points is never large, so we perform a nearest-neighbors averaging in order to smooth the friction and facilitate the computation of its curl, which appears in Eq. (15).

VII. RESULTS AND DISCUSSION

We have performed a number of numerical experiments in which we have computed the self-consistent decay of arbitrary initial vortex tangles and ABC flow configurations. Each run is characterized by the amplitude A^* of the initial ABC flow, the vortex line density L^* of the initial tangle, and the temperature T. The temperature determines the dimensionless friction coefficient α, the dimensionless quantum of circulation Γ, and the density ratio ρ_s/ρ_n. Because of the lack of external forcing, all calculations result in the decay to zero of both the motion of the normal fluid and of the vortex line density. What interests us is how and at which

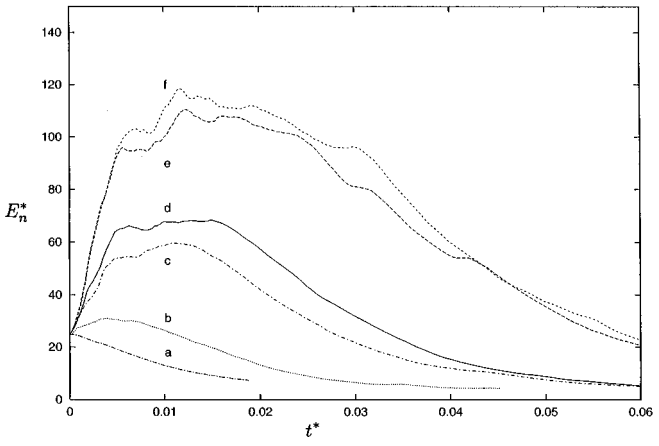

FIG. 4. Dimensionless normal-fluid density E_n^* vs dimensionless time t^* for different runs (see Table I) starting with $A=5$.

rate this decay takes place. We concentrate our attention onto the normal fluid because very little is known (apart from the linear calculation of Ref. 19) about the effect which the vortices have on the normal fluid.

A global quantity which is particularly interesting is the energy E_n contained in the normal fluid

$$E_n=\frac{\rho_n}{2}\int_{-\lambda/2}^{\lambda/2}dx\int_{-\lambda/2}^{\lambda/2}dy\int_{-\lambda/2}^{\lambda/2}dz(\mathbf{v}_n)^2. \tag{25}$$

In dimensionless form we have

$$E_n^*=\frac{E_n}{\rho_n\nu_n^2\lambda}=\frac{1}{2}\int_{-1/2}^{1/2}dx^*\int_{-1/2}^{1/2}dy^*\int_{-1/2}^{1/2}dz^*(\mathbf{v}_n^*)^2. \tag{26}$$

Figures 4 and 5 show how E_n^* decays as a function of the dimensionless time t^*. The initial vortex tangle is the same in all cases ($L^*=29.5$), and the initial ABC flow has amplitude $A^*=5$ in Fig. 4 and $A^*=13.6$ in Fig. 5. Note that the values of A^* chosen are well below the threshold of the Glaberson instability: if the density of the vortex tangle increased, we would need more points to represent the vortex lines, and the computation of the Biot-Savart law would become unacceptably slow. The calculations are performed at a number of different temperatures, from the lambda region down to $T=2.0\,\mathrm{K}$, the parameters used in each run being listed in Table I.

TABLE I. Parameters used in the runs showed in Figs. 4 and 5.

run	T (K)	A^*	E_n^*/E_s^*	$E_n^*(t^*)$
a	2.171	5	1.19	drops
b	2.16	5	0.21	rises
c	2.12	5	0.06	rises
d	2.10	5	0.05	rises
e	2.02	5	0.02	rises
f	2.0	5	0.02	rises
g	2.171	13.6	8.78	drops
h	2.16	13.6	1.55	drops
i	2.15	13.6	0.99	drops
j	2.14	13.6	0.74	drops
k	2.12	13.6	0.48	rises
l	2.10	13.6	0.34	rises
m	2.05	13.6	0.21	rises

It is apparent from Figs. 4 and 5 that a variety of decay behavior is possible, depending on the parameters chosen. The general feature (summarized by the last column of Table I) is that at the higher temperatures the normal fluid decays immediately, while at intermediate and lower temperatures the normal-fluid energy $E_n^*(t^*)$ rises from its initial value $E_n^*(0)$ to a maximum value $E_{n,\max}^*$ before decaying. The effect is more pronounced at $A^*=5$ than at $A^*=13.6$. On the contrary, the superfluid vortex tangle's density L^* decays monotonically in all runs; see Fig. 6.

To understand the initial rise of E_n^* we compare the initial ratio of the energies of the normal fluid and the superfluid. In the first approximation the energy contained in the tangle is simply

$$E_s\approx\epsilon_s L\lambda^3, \tag{27}$$

where

$$\epsilon_s=\frac{\rho_s\kappa^2}{4\pi}\ln\left(\frac{b}{a_0}\right) \tag{28}$$

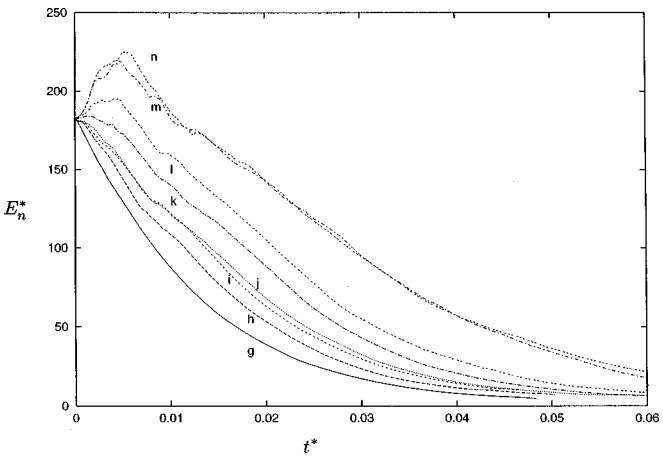

FIG. 5. Dimensionless normal-fluid density E_n^* vs dimensionless time t^* for different runs (see Table I) starting with $A=13.6$.

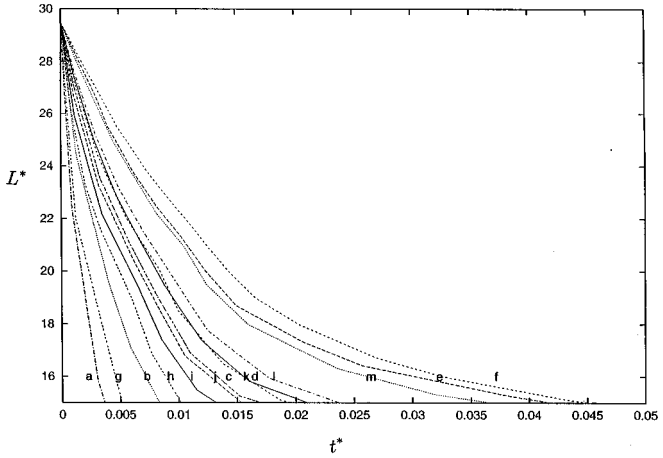

FIG. 6. Vortex line density L^* vs time t^*. The labels under each curve refer to Table I.

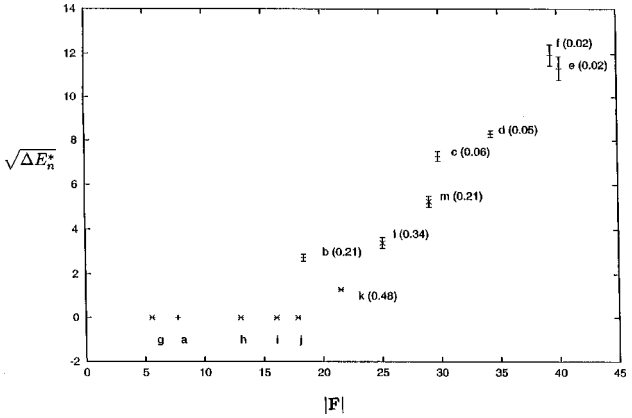

FIG. 7. Dimensionless energy increase $\sqrt{\Delta E_n^*}$ vs dimensionless drive $|\mathbf{F}|$ of different runs. The labels refer to Table I. The figures in bracket represent E_n^*/E_s^*.

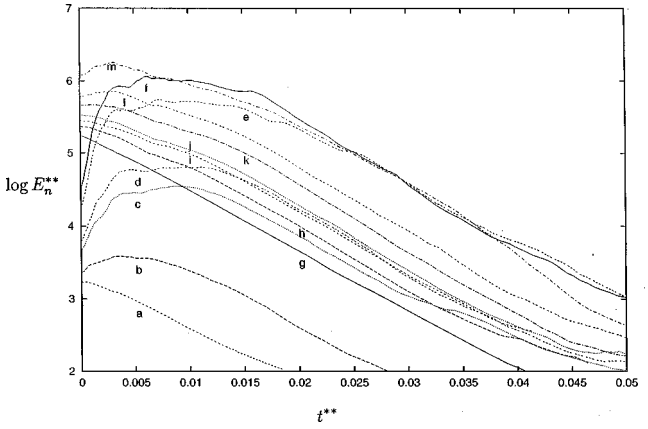

FIG. 8. Decay of normal-fluid energy $\ln(E_n^{**})$ vs t^{**} for different runs, where energy and time are measured in terms of viscous diffusion times of the *total* helium density ρ.

is the energy per unit length of vortex line and $b \approx L^{-1/2}$ is the average intervortex spacing. In dimensionless units we have then

$$E_s^* = \frac{E_s}{\lambda \rho_n \nu_n^2}. \tag{29}$$

Table I lists the ratio E_n^*/E_s^* at the beginning of each run. It is apparent from Figs. 4 and 5 and Table I that a rise of E_n^*, that is to say a transfer of energy from the superfluid to the normal fluid, occurs only if at $t^*=0$ we have $E_s^* > E_n^*$. From the data of Table I this is thus a necessary, though not sufficient, condition.

What determines quantitavely how much energy stored in the tangle is transferred to the normal fluid depends on the actual mutual friction coupling $\mathbf{F}$ [Eq. (18)]. The coupling is proportional to the integrated mismatch of normal fluid and superfluid velocities. A simple way to estimate the magnitude of the initial $\mathbf{F}$, and hence predict whether E_n^* will rise or not, is to compute $|\mathbf{F}| \approx \alpha \Gamma \rho_s/\rho_n L^* \Delta v^*$ where Δv^* is the difference between the initial maximum velocity of the normal fluid (which is $2A$ by construction) and the initial maximum velocity of the superfluid (given by the highest contour level of Fig. 3, for example). Figure 7 shows that the energy increase $\sqrt{\Delta E_n^*}$ where $\Delta E_n^* = E_{n,\max}^* - E_n^*(0)$ is proportional to $|\mathbf{F}|$, and the data are essentially ordered by the ratio E_n^*/E_s^*. We conclude that it is the initial mutual friction force that actually determines the evolution of the normal fluid. From the picture it appears that the initial mutual friction forcing must be higher than a critical value before E_n^* is increased: what happens in runs a,g,h,i, and j is that the energy E_n^* either decreases immediately or holds its value for a time lag before decreasing, but never increases.

The possibility that energy stored in the vortex tangle is transfered to the normal fluid was discussed by Schwarz and Rosen[27] to explain their measurements of the free decay of quantized vortex lines in a channel. They observed two distinct stages of decay: an initial rapid decay followed by a slower one. They claimed that the first stage of decay is consistent with the known vortex dynamics model of Schwarz and Vinen's phenomenological equation.[28] The second, slower stage of decay, according to Schwarz and Rosen, was a self-consistent coupled decay regime in which energy is transferred from the superfluid to the normal fluid through the mutual friction and then dissipated through viscosity, and the rate of decay is no longer dominated by quantized vortex dynamics but by normal-fluid viscous effects. Schwarz and Rosen argued that the second stage is a regime of coupled turbulence in which the normal fluid and the superfluid evolve self-consistently. They analyzed the data using a simple one-dimensional model and they concluded that the second stage of decay takes place when energy initially stored in the superfluid flows into the normal fluid. Our finding illustrates Schwarz and Rosen's interpretation.

Past the initial rise of Figs. 4 and 5, the normal-fluid energy decreases, and it is interesting to consider the rate at which this decay takes place. It is important to appreciate that in the curves of Figs. 4 and 5 the unit of time λ^2/ν_n actually changes from run to run, depending on the temperature. We introduce a viscous diffusion time scale λ^2/ν where $\nu = \mu/\rho$ is a kinematic viscosity based on Helium's *total* density ρ rather than on the normal-fluid density ρ_n. Correspondingly, we now have units of speed λ/ν and energy $\lambda \nu^2 \rho_n$ at the place of λ/ν_n and $\lambda \nu_n^2 \rho_n$. We use a double star to denote the scaling of the variables and in Fig. 8 we plot the decay of the normal fluid energy $E_n^{**} = E_n/(\lambda \nu^2 \rho)$ as a function of the time $t^{**} = t\nu/\lambda^2$. Since in the absence of vortex lines the normal fluid would decay exponentially, we plot the natural logarithm of E_n^{**}, so the slope gives directly the decay constant.

The figure shows that *all* runs decay exponentially after an eventual initial rise, and, more important, the decay rate just after that rise is the same. After the eventual initial rise, the normal-fluid energy E_n^{**} drops like $\exp(-\sigma t^{**})$ with decay constant σ approximately in the range $-79 \leqslant \sigma \leqslant -83$ (it is difficult to define σ more precisely because of the arbitrariness in defining the fitting region, after the initial transient and before the vortex line density is too low). This uniform value of the decay constant is at first surprising: how does the normal fluid know about the *total* helium density? Note that the temperature range covered by the results corresponds to a normal-fluid fraction ρ_n/ρ which varies be-

tween 99% at $T=2.171\,\mathrm{K}$ and only 56% at $T=2.0\,\mathrm{K}$. In the absence of a tangle the energy of the normal ABC flow should drop like $\exp[-8\pi^2(\rho/\rho_n)t^{**}]$, that is to say the decay rate should change from $\sigma=-79$ at the lambda point to $\sigma=-141$ at $T=2.0\,\mathrm{K}$, almost doubling its value. The data clearly show that this change does not happen. The interpretation of the data is that the coupling between the normal fluid and the tangle is strong enough to compensate for the changing relative proportion of normal fluid. Although our model is too idealized to make a direct quantitative comparison with the experiments, our result is consistent with the observation by Stalp[5,6] that the decay rate of helium turbulence is independent of temperature. Note that the actual decay rate which we calculate cannot be compared with Stalp's measurements, since in our case we have the exponential decay of an ABC flow and in his case there is the power-law decay of more complex isotropic turbulence.

The observed decay rate of L^*, on the contrary, does not follow any simple scaling rule. This is not totally unexpected since the tangle is forced by an anisotropic, hence somewhat artificial, two-dimensional normal fluid. This suggests that it will be important in the future, when more computer power is available, to couple the superfluid tangle to a three-dimensional normal fluid.

VIII. CONCLUSIONS

We have identified the limitation of the existing theoretical approach to study the turbulence of helium II: that it neglects the back reaction of the superfluid vortex lines onto the normal fluid. We have proposed an approach to study the coupled evolution of normal fluid and vortex lines. Its key feature is that it is dynamically self-consistent. We have implemented this approach to study a rather idealized model of decay of a two-dimensional normal-fluid eddy coupled to a three-dimensional vortex tangle.

Despite the simplicity of our model, we have been able to recognize physical effects which have been observed and discussed in the experimental literature. The first effect is the transfer of energy from the vortex tangle to the normal fluid and the viscous decay of the normal fluid coupled to the tangle. This effect has been discussed by Schwarz and Rosen[27] to interpret their measurements, and our result confirm their observation.

The second effect which we have found is that energy decay rates are independent of temperature. It appears that the friction coupling with the tangle is large enough to compensate for the decreasing proportion of normal fluid at lower temperatures. This effect is in qualitative agreement with the experiments of Stalp.[5,6]

Further work will attempt to go beyond the simplicity of the current model. At the moment the major limitation is the computer power available, which forces us to use a rather low-density vortex tangle and restrict the study to two-dimensional normal flows. The aim will be to perform the calculation with a three-dimensional normal fluid and a much higher vortex line density L^*. This will allow us to investigate what should be the best way to perform the averaging process in the calculation of **F**: ideally one would like to obtain the HVBK limit; another issue is whether there is a scaling law for the decay of L^*, which we have not found with our simplified model. A fully three-dimensional calculation would also allow us to study forced turbulence and compute energy spectra to compare with the experiment of Maurer and Tabeling.[7]

ACKNOWLEDGMENT

This work was supported by a Royal Society equipment grant.

*Electronic address: C.F.Barenghi@ncl.ac.uk
†Electronic address: D.C.Samuels@ncl.ac.uk

[1] P. L. Walstrom, J. G. Weisend, J. R. Maddocks, and S. W. VanSciver, Cryogenics **28**, 101 (1988).
[2] H. Borner, T. Schmeling, and D. W. Schmidt, Phys. Fluids **26**, 1410 (1983).
[3] F. Bielert and G. Stamm, Cryogenics **33**, 938 (1993).
[4] M. R. Smith, R. J. Donnelly, N. Goldenfeld, and W. F. Vinen, Phys. Rev. Lett. **71**, 2583 (1993).
[5] S. Stalp, Ph.D. thesis, University of Oregon, 1998.
[6] S. Stalp, L. Skrbek, and R. J. Donnelly (unpublished).
[7] J. Maurer and P. Tabeling, Europhys. Lett. **43**, 29 (1998).
[8] D. C. Samuels and R. J. Donnelly, Phys. Rev. Lett. **65**, 187 (1990).
[9] C. F. Barenghi, R. J. Donnelly, and W. F. Vinen, J. Low Temp. Phys. **52**, 189 (1983).
[10] R. J. Donnelly, *High Reynolds Number Flows Using Liquid and Gaseous Helium* (Springer Verlag, New York, 1991).
[11] K. W. Schwarz, Phys. Rev. Lett. **49**, 283 (1982); Phys. Rev. B **31**, 5782 (1985); **38**, 2398 (1988).
[12] J. Koplik and H. Levine, Phys. Rev. Lett. **71**, 1375 (1993).
[13] R. L. Ricca, D. C. Samuels, and C. F. Barenghi, J. Fluid Mechanics (to be published).
[14] D. C. Samuels, Phys. Rev. B **46**, 11 714 (1992).
[15] R. G. K. Aarts and A. T. A. M. deWaele, Phys. Rev. B **50**, 10 069 (1994).
[16] H. Penz, R. G. K. Aarts and A. T. A. M. deWaele, Phys. Rev. B **51**, 11 973 (1995).
[17] D. C. Samuels, Phys. Rev. B **47**, 1107 (1993).
[18] C. F. Barenghi, D. C. Samuels, G. H. Bauer, and R. J. Donnelly, Phys. Fluids **9**, 2631 (1997).
[19] D. J. Melotte and C. F. Barenghi, Phys. Rev. Lett. **80**, 4181 (1998).
[20] H. E. Hall and W. F. Vinen, Proc. R. Soc. London, Ser. A **238**, 215 (1954); R. N. Hills and P. H. Roberts, Arch. Ration. Mech. Anal. **66**, 43 (1977); I. M. Khalatnikov, *An Introduction to the Theory of Superfluidity* (Benjamin, New York, 1996).
[21] C. F. Barenghi, Phys. Rev. B **45**, 2290 (1992); K. L. Henderson, C. F. Barenghi, and C. A. Jones, J. Fluid Mech. **283**, 329 (1995).
[22] Y. B. Zeldovich, A. A. Ruzmaikin, and D. D. Sokoloff, *Magnetic Fields in Astrophysics* (Gordon and Breach, New York, 1983).
[23] D. R. Fearn, P. H. Roberts, and A. M. Soward, in *Energy, Stability and Convection*, edited by G. P. Galdi and B. Straughan (Longmans, New York, 1988).
[24] T. Dombre, U. Frisch, J. M. Greene, M. Henon, A. Mehr, and A. M. Soward, J. Fluid Mech. **167**, 353 (1986).

[25] A. D. Gilbert and S. Childress, *Stretch, Twist, Fold: The Fast Dynamo* (Springer, Berlin, 1995); D. J. Galloway and M. R. E. Proctor, Nature (London) **356**, 691 (1992).
[26] G. Pfister, H. Schmidt, K. A. Cliffe, and T. Mullin, J. Fluid Mech. **191**, 1 (1988).
[27] K. W. Schwarz and J. R. Rosen, Phys. Rev. Lett. **66**, 1898 (1991).
[28] W. F. Vinen, Proc. R. Soc. London, Ser. A **240**, 114 (1957); **240**, 128 (1957); **242**, 493 (1957); **243**, 400 (1957).